

Article

Topography Control of Micro-Nanosized Anatase Coating on Magnesium Alloy

Shusen Hou ^{1,2,*}, Tingting Yang ², Yue Li ^{2,*}, Liming Lian ², Weixin Yu ² and Lin Yang ¹

¹ School of Chemistry and Chemical Engineering, Henan Normal University, Xinxiang 453007, China; yanglin1819@163.com

² School of Mechanical and Electrical Engineering, Xinxiang University, Xinxiang 453003, China; yangtingting@xxu.edu.cn (T.Y.); lianliming@xxu.edu.cn (L.L.); yuweixin@xxu.edu.cn (W.Y.)

* Correspondence: shusenh@163.com (S.H.); liyue@xxu.edu.cn (Y.L.)

Abstract: Constructing surface topographies in the micro- or nanometer range is an effective way to improve the biocompatibility of biomaterials. For the present work, anatase coatings with controllable micro/nanoscale characteristics were successfully prepared on an MgZn alloy surface via solvothermal route, and their formation mechanisms are discussed. The features of the as-prepared coatings were characterized using a scanning electron microscope (SEM), a transmission electron microscope (TEM), an atomic force microscope (AFM), X-ray diffraction (XRD), and a contact angle goniometer. The corrosion behavior of the coatings was also evaluated by testing the open circuit potential (OCP) in SBF (Simulated Body Fluid). The results show that a gradual variation of the anatase coating morphologies was obtained through adjusting the solvothermal reaction conditions. With the increase of NH₄F concentration in the solution, the cross-combined anatase nanosheets became more dispersed. The micro/nanostructured anatase coatings provide the MgZn alloy with good corrosion resistance, which increased with the density of anatase nanosheets in the coatings. In addition, the coatings exhibit the inhibition of platelet aggregation, and the micro/nano structures can also adsorb endothelial cells.

Keywords: topography; micro/nanostructure; anatase; coating; magnesium alloy



Citation: Hou, S.; Yang, T.; Li, Y.; Lian, L.; Yu, W.; Yang, L. Topography Control of Micro-Nanosized Anatase Coating on Magnesium Alloy. *Coatings* **2022**, *12*, 1063. <https://doi.org/10.3390/coatings12081063>

Academic Editor: Gabriela Ciobanu

Received: 3 June 2022

Accepted: 22 July 2022

Published: 27 July 2022

Publisher's Note: MDPI stays neutral with regard to jurisdictional claims in published maps and institutional affiliations.



Copyright: © 2022 by the authors. Licensee MDPI, Basel, Switzerland. This article is an open access article distributed under the terms and conditions of the Creative Commons Attribution (CC BY) license (<https://creativecommons.org/licenses/by/4.0/>).

1. Introduction

1.1. Background

Biomedical metal, such as stainless steel, titanium alloy, and cobalt-based alloy, have been widely used in orthopedic, cardiovascular, and dental fields because of their high strength and corrosion resistance [1,2]. However, these metal materials are chemically stable in the human physiological environment. Sometimes they need to be removed by secondary surgery, which undoubtedly increases the pain and medical expenses of patients. As an implant material, biomedical magnesium alloy has good biocompatibility, and is easily corroded and destroyed in the physiological environment until it disappears completely. Its degradation products can be metabolized and absorbed by the human body, and thus secondary surgery can be avoided. Therefore, magnesium alloys, as biodegradable and absorbable biomedical materials, have attracted much attention in bone tissue repair and cardiovascular therapy, and have become a hot issue in the field of biomaterials [3,4].

Studies have shown that magnesium alloys corrode too fast in the physiological environment, which leads to a sharp decline in the stability of their structure and properties. In this case, stable support could not be provided in the process of tissue repair, since it may lead to the premature failure of implants. Proper surface modification of the magnesium alloy could control the degradation rate and improve biocompatibility [5–7]. The most common surface modification method is to produce protective coatings on magnesium alloys, which mainly include some inorganic coatings and degradable polymer coatings [8].

For example, in bone fixation implants field, hydroxyapatite (HA), one of the primary constituents of bone, has been extensively prepared onto magnesium alloy substrates by different methods. In many cases, HA coatings could slow down the corrosion rate and improve the biocompatibility or osseointegration of magnesium alloy implants [9,10].

In the field of magnesium alloy cardiovascular stents, some organic-based coatings have been employed as corrosion protection layers, or more importantly, as drug delivery carriers to prevent in-stent restenosis (ISR) [11–13]. On the other hand, as an inorganic material, titanium dioxide was gradually used to prepare the protective coating of magnesium alloy stents, aiming to provide increased corrosion resistance and improved biocompatibility of magnesium alloys [14–16].

It is generally believed that the optimal surface of cardiovascular implants should be blood compatible, and moreover, promote the adhesion and growth of endothelial cells (ECs), while suppressing the adhesion and proliferation of smooth muscle cells (SMCs). Building a monolayer of endothelial cells on the stents is considered to be the most efficient approach to reducing the risk of clot formation and restenosis, because an anticoagulant surface can be offered by the endothelial layer [17,18]. So, it is vital for stents to enhance the adherence, migration, and proliferation of ECs, resulting in rapid re-endothelialization after cardiac interventional therapy.

1.2. The Purpose of the Research

As is well known, the surface topography of biomaterial with micro- or nano- characteristics could play a critical role in cell adhesion and proliferation [17,19,20]. Hence, it is possible to fabricate specific surface microstructures on magnesium alloy stents to enhance the re-endothelialization, thus preventing the formation of ISR [21,22]. In our early research, anatase titanium dioxide coatings with flower-like and sheet-like structures were prepared on MgZn alloys for vascular stent application, since the titanium oxide films have excellent blood compatibility [23,24]. We believe that an intensive study is necessary to precisely control the structures and topographies of anatase coatings in micro/nanometer range. In this paper, gradually varying surface topographies provided by anatase coatings were constructed on MgZn alloy substrates by adjusting the solvothermal reaction conditions. The formation mechanism and properties of the coatings are discussed below.

2. Materials and Methods

2.1. Coating Preparation

In this study, anatase coatings were fabricated on an MgZn alloy (composition: 2.0 wt.% Zn, 0.5 wt.% Nd, 0.46 wt.% Y, and balance Mg), developed by Zhengzhou University, Zhengzhou, China [25]. Samples with dimensions of $15 \times 10 \times 3 \text{ mm}^3$ were cut from the as-cast ingots by wire-electrode machining, mechanically polished, and sonicated in ethanol. Then, they were stored in ethanol before being solvothermal-treated in a Teflon vessel.

Solvothermal treatment was carried out in Teflon-lined stainless-steel autoclave, in which 18 mL absolute alcohol and 140 μL titanium butoxide (TBOT) were employed as solvent and reactant, respectively. To obtain micro/nano anatase coatings on the MgZn samples, 70 μL hydrofluoric acid (HF, 40 wt.%) and 140 μL NH_4F aqueous solution (0.1–0.3 M) were successively added into the former solution. After being stirred for 10 min, the Teflon vessel containing the mixed solution and upright samples was sealed and fixed in the autoclave, then treated at 170 °C for 12 h. Subsequently, the autoclave was cooled, and the samples were taken out from the Teflon vessel, cleaned ultrasonically in deionized water, then dried. In this study, for simplicity, abbreviations for the samples with different coatings are listed in Table 1.

2.2. Coating Characterization

The surface characteristics were observed by a scanning electron microscope (SEM, SU8000, Hitachi, Tokyo, Japan), an atomic force microscope (TEM, Talos F200X, FEI, Hills-

boro, OR, USA), and an atomic force microscope (AFM, MultiMode8, Bruker, Billerica, MA, USA). To obtain the cross-section image, the coating was slightly scratched with a sharp blade, and the coating was partially damaged and broken away from the substrate, in order to find the cross-section morphology under a scanning electron microscope. For TEM analysis, a small number of powders was carefully scraped from the coatings and dispersed in ethanol, and the dispersion was dropped on carbon-copper grids and dried. The crystal structure of the coatings was determined through X-ray diffraction (XRD, X'Pert3 Powder, PANalytical, Malvern, UK) with Cu K α radiation at 45 kV and 40 mA. The water contact angle (CA, $n = 3$) was measured with 10 μ L droplets of deionized water employing a contact angle meter.

Table 1. List of the abbreviations used in this paper.

No.	Abbreviation	Sample Description
1	MgZn	Bare MgZn substrate
2	MgZn-0.1 F	MgZn substrate with anatase coating, prepared in solution containing 140 μ L of 0.1 M-NH ₄ F aqueous solution
3	MgZn-0.2 F	MgZn substrate with anatase coating, prepared in solution containing 140 μ L of 0.2 M-NH ₄ F aqueous solution
4	MgZn-0.3 F	MgZn substrate with anatase coating, prepared in solution containing 140 μ L of 0.3 M-NH ₄ F aqueous solution

2.3. Corrosion Resistance Tests

The corrosion resistance tests of the bare and coated MgZn samples were conducted on an electrochemical station (CS2350, Wuhan Corrtest Instrument Co., Ltd. Wuhan, China) with a three-electrode cell in which the sample, platinum electrode, and saturated calomel electrode were the working, counter, and reference electrodes, respectively. Electrochemical measurements were performed at 37 °C in simulated body fluid (SBF), based on Ref. [26].

2.4. Biocompatibility Evaluation

In this paper, biocompatibility was evaluated including the platelets and endothelial cells adhesion. For the platelets adhesion test, fresh human anticoagulant blood was centrifuged at 1500 rpm for 15 min, then the upper yellow liquid was separated to obtain platelet-rich plasma (PRP). An amount of 0.5 mL of PRP was dropped into 24-well culture plates containing samples, and incubated at 37 °C for 1 h. Then, the samples were rinsed with normal saline and fixed with glutaraldehyde. After that, samples were dehydrated in increasing concentrations of ethanol, successively. Human umbilical vein endothelial cells (HUVECs, Ea.hy926) were used to observe the cells adhesion to the samples. Firstly, the sterilized samples were put into 24-well culture plates, then the endothelial cells were seeded on the samples under a concentration of 2×10^4 cells/mL. After a 24 h incubation period, the samples were washed with PBS buffer then treated by PBS buffer containing 2.5% glutaraldehyde for 12 h, and dehydrated with 50%, 75%, 90%, and 100% ethanol. The samples were dried, then the platelets and cells were observed by SEM.

3. Results and Discussion

3.1. Coating Characteristics

The surface morphologies of the MgZn-0.1 F, MgZn-0.2 F and MgZn-0.3 F are presented in Figure 1. All samples were prepared by solvothermal treatment at 170 °C for 12 h in the mixed solution of alcohol, TBOT, HF, and NH₄F. The only different parameter is the NH₄F concentration, varying from 0.1–0.3 M as described in the Experimental section. Figure 2 indicates the XRD patterns of the samples. Clearly, in each sample there were two phases detected: the MgZn phase as the substrate and the anatase phase (PDF#21-1271) as the surface coating. Figure 1 shows that the surface of every sample was composed of anatase sheets. However, the coatings were significantly different in topographies, reflected in the crystal size, density, as well as conglomeration state of the anatase microstructures. At a lower NH₄F concentration (i.e., 0.1 M), the coating was very dense due to the high degree of aggregation of the layer-by-layer anatase sheets. These aggregates were crossed and interconnected with each other. There was hardly any porosity in this coating, as

shown in Figure 1a,d. With the increase of NH_4F concentration, the number and size of anatase sheets in the aggregates decreased notably. Moreover, porous morphologies appeared in the coatings because the sheet-like aggregates were dispersing gradually, as shown in Figure 1b,c,e,f.

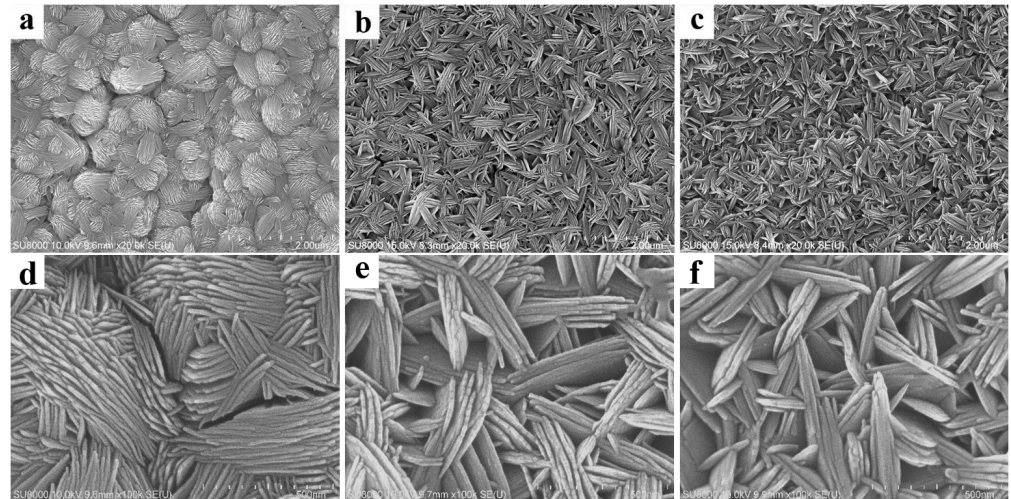


Figure 1. SEM surface morphologies of anatase coatings: (a,d) MgZn-0.1 F; (b,e) MgZn-0.2 F; (c,f) MgZn-0.3 F.

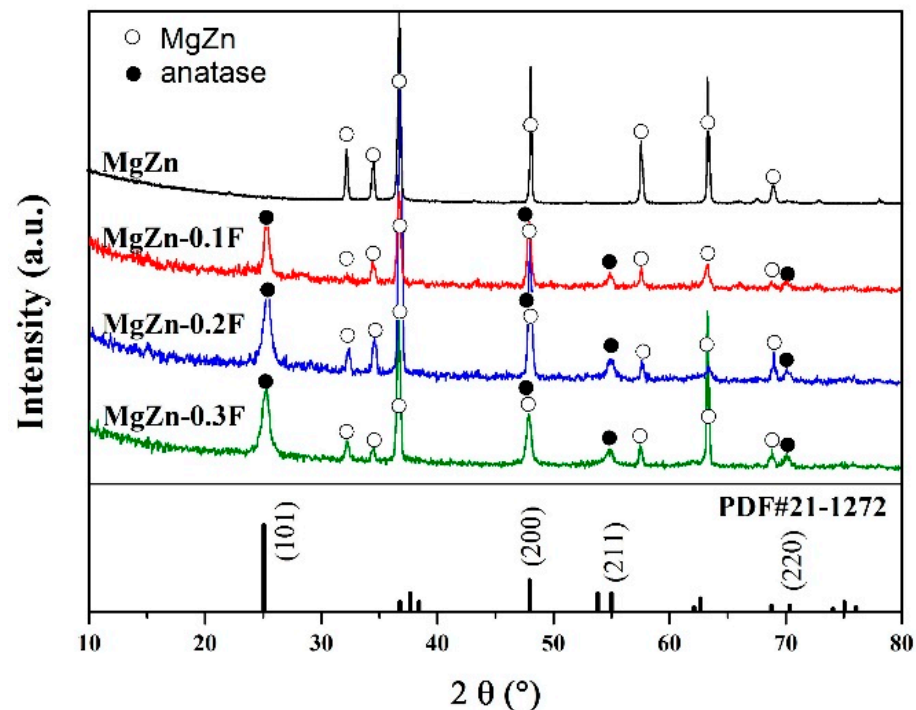


Figure 2. XRD patterns of the as-prepared anatase coatings.

Figure 3a shows the TEM image of a broken anatase aggregate partially scraped from the surface of the MgZn-0.3 F sample. It confirms that the aggregates were assembled from anatase nanosheets with a thickness of 10–20 nm. These nanosheets were parallel or crossed with each other during the growth process. As seen in Figure 1c,f, the aggregates of these nanosheets were significantly larger than 100 nm, close to micron scale. So, we defined the coating as a micro/nano-scale structure coating. In Figure 3b, the High-resolution TEM

image shows the (004) planes of anatase with a crystal plain spacing of 0.237 nm, which indicates that the top and bottom surfaces of the anatase sheets are (001) planes.

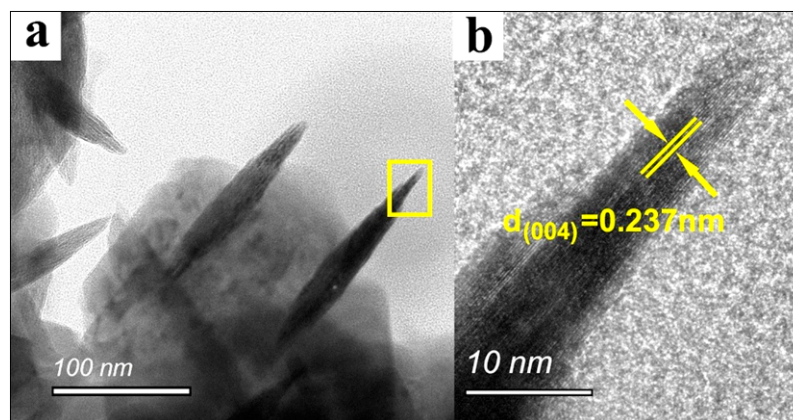


Figure 3. (a) TEM image of the of the anatase sheets; (b) high-resolution TEM image of the edge of a single anatase sheet selected in the rectangle region in (a).

3.2. Formation Mechanism of the Coatings

The above results demonstrate that the different morphologies of the as-prepared anatase coatings are strongly dependent on the NH_4F concentration in the solvothermal solution. After a 12 h solvothermal treatment, we can obtain a complete coating with a final thickness of 750 nm (Figure 4). In order to reveal the underlying causes of the difference in topographies, two samples were prepared by solvothermal treatment at 170 °C for 6 h in solutions containing 0.1 M- NH_4F and 0.2 M- NH_4F , separately. This is because after a shorter time of 6 h, some evolving information of the coating can emerge. In Figure 5, it can be seen that both coatings present a layered characteristic, i.e., the anatase sheets or their aggregates in the upper layer, and lots of blocks in the bottom layer. The nano-scale thin sheets were parallel or cross-combined, and developed into the aggregates. On the basis of the XRD results in Figure 2, we conclude that the blocks were also anatase crystals, the same as the nano-thin sheets. However, there as an obvious difference in the surface morphologies of the two samples. For the MgZn-0.2 F sample, the anatase blocks are bigger in size and have more regular shapes, and the number of the sheet aggregates is less than that of the MgZn-0.1 F sample.

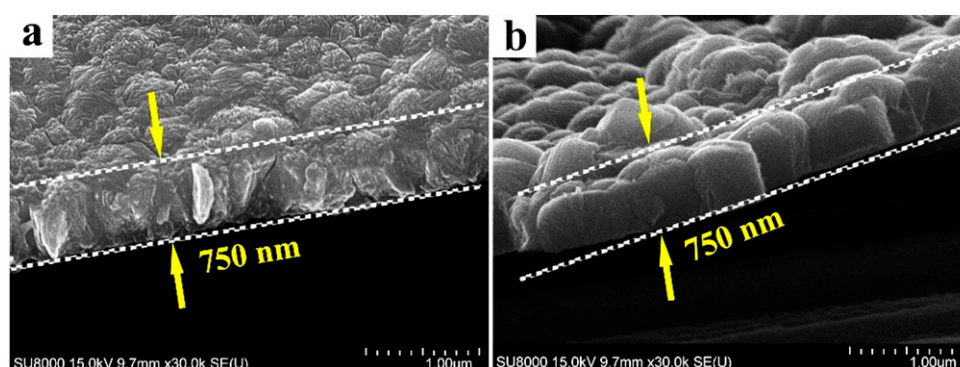


Figure 4. Cross-section morphologies of anatase coatings grown at 170 °C for 12 h in solutions containing: (a) 18 mL alcohol, 140 μL TBOT, 70 μL HF, 140 μL NH_4F (0.1 M); (b) 18 mL alcohol, 140 μL TBOT, 70 μL HF, 140 μL NH_4F (0.2 M).

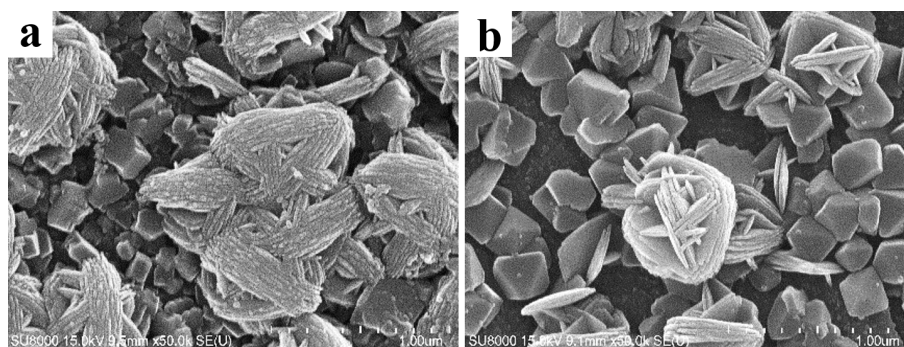


Figure 5. SEM morphologies of anatase coatings grown at 170 °C for 6 h in solutions containing: (a) 18 mL alcohol, 140 μ L TBOT, 70 μ L HF, 140 μ L NH_4F (0.1 M); (b) 18 mL alcohol, 140 μ L TBOT, 70 μ L HF, 140 μ L NH_4F (0.2 M).

From the cross-section morphologies in Figure 4, it is found that both the MgZn–0.1 F and MgZn–0.2 F coatings have the same thickness of about 750 nm after a 12 h hydrothermal reaction. However, the former coating has a rougher cross-section than the latter, and no blocks can be found within the whole cross-section of the former coating. Hence, we infer that the anatase blocks were almost entirely converted into anatase sheets from 6 h to 12 h during the hydrothermal reaction. For the latter coating, some anatase blocks, less than that of the same one prepared after a 6 h hydrothermal reaction, can still be seen in the cross-section (see Figures 4b and 5b). It could be concluded that during the anatase coating formation process, the anatase crystals were evolved from block-like to sheet-like, and the conversion process was slower when the hydrothermal reaction was conducted in solution with the higher NH_4F concentration.

Generally, anatase crystals are dominated by the {101} planes, causing them to exhibit the double-pyramidal appearance [27]. In Figure 5b, it can be seen that the anatase crystals at the bottom have a pyramidal shape, which are consistent with other studies. In fact, in this paper, NH_4F has important effects on the crystal growth of anatase crystals. Firstly, adequate fluorine ions (F^-) were supplied by the hydrolysis of NH_4F , and these fluorine ions can be absorbed onto the surfaces of the anatase planes, markedly reducing the surface energy of the {001} planes to a level lower than that of the {101} planes, making the {001} planes more stable than the {101} planes [28]. So, the anatase crystal with exposed {001} planes can be achieved during its growth process, which led to the plate-like appearance. Secondly, it is found that the anatase crystals have a slower growth rate under a higher NH_4F concentration. In our previous research, it has been confirmed that the growth of anatase crystals would slow down when the HF amount was increased, because low pH would suppress the hydrolysis of TBOT [23]. However, in this current study the HF content is constant (70 μ L) for all the solvothermal treatment conditions. So, we think the slower growth rate of the anatase crystals (or the formation of the anatase coating) may be attributed to the slight adjustment of pH by the hydrolysis of NH_4F . This is because the aqueous solution of NH_4F is weakly acidic.

3.3. Properties of the Coatings

The surface roughness and wettability of biomaterials have an important influence on cell adhesion and growth [29]. Herein, atomic force microscopy (AFM) was used to measure the roughness of the anatase coatings, as well as to observe their surface topographies in detail. The AFM images of MgZn–0.1 F, MgZn–0.2 F, and MgZn–0.3 F are shown in Figure 6a–c. The AFM micrographs agreed well with the SEM results in Figure 1, and indicated a rougher surface for the MgZn–0.3 F sample with a roughness (R_a) of 90.1 nm. On the other hand, both the MgZn–0.1 F and MgZn–0.2 F samples showed a smoother surface with R_a values of 49.7 and 53.8 nm, respectively. The results showed that the surface roughness of the coatings increased with the concentration of the NH_4F . In addition,

lower density of the anatase nanosheets were clearly observed in the surface of MgZn-0.2 F and MgZn-0.3 F samples. Furthermore, the contact angle of the sample surface with deionized water was tested to assess the surface wettability. The contact angles of the MgZn substrate [14], MgZn-0.1 F, MgZn-0.2 F, and MgZn-0.3 F were 8.4° , 13.02° , 17.14° , and 16.73° , as shown in Figure 6d–f. The results indicated that the anatase-coated samples were hydrophilic, and there was no significant difference in wettability between the anatase-coated samples.

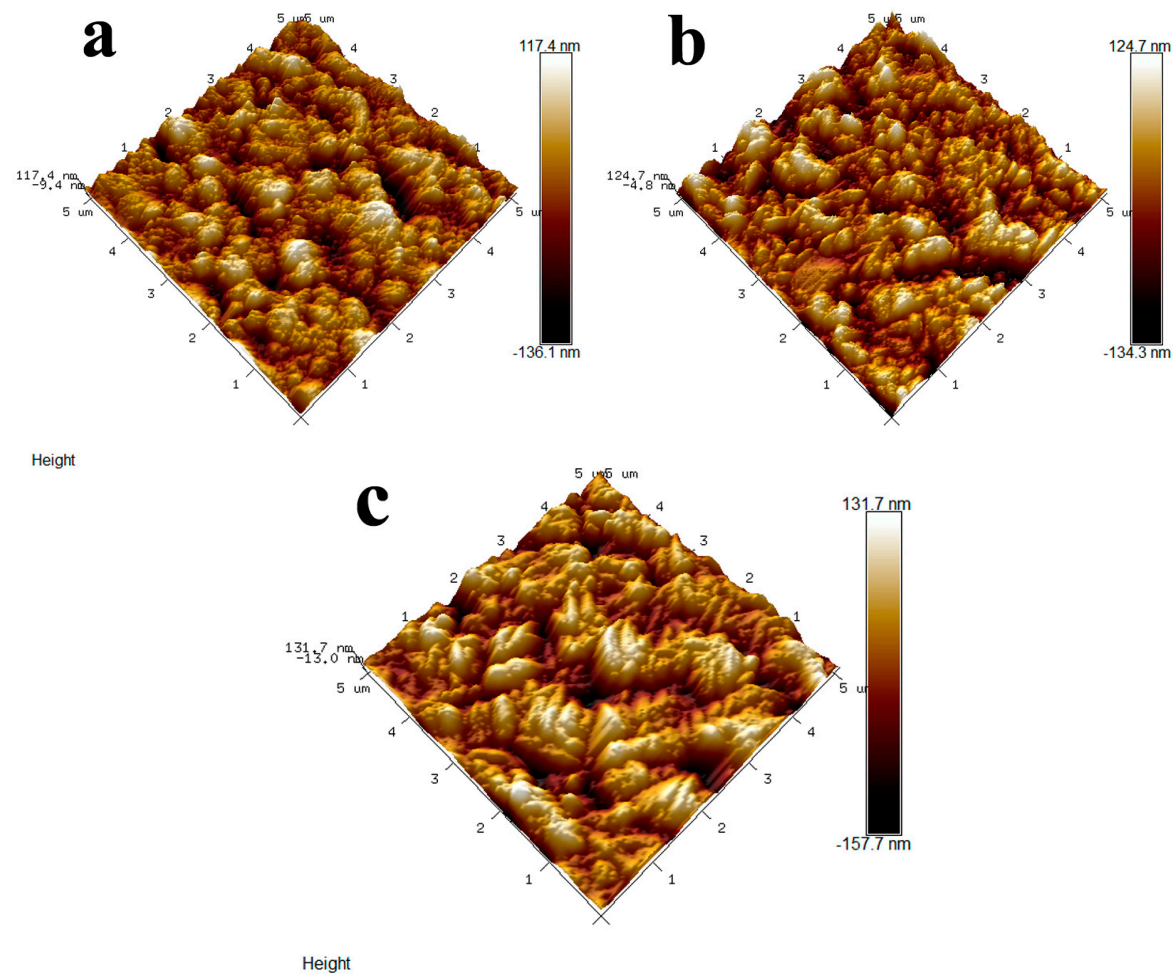


Figure 6. AFM micrographs and contact angles of the anatase coatings: (a,d) MgZn-0.1 F; (b,e) MgZn-0.2 F; (c,f) MgZn-0.3 F.

Open-circuit potential (OCP) was used to monitor the chemical stability and estimate the corrosion tendency of the samples. Figure 7 shows the OCP curves in SBF of the anatase-

coated and uncoated samples. For the uncoated MgZn substrate, the open-circuit potential increased continuously in the initial period, and then gradually decreased to a stable value of -1.756 V during 20 min immersion. When the bare MgZn sample was immersed in the SBF, a film of corrosion products began to grow on its surface and acted as a protective layer to increase the potential. Then, the products damaged and broke away from the sample surface to decrease the potential. The damage of the previous products and the formation of the new products gradually reached a dynamic equilibrium. However, the OCP values of all anatase-coated MgZn samples were decreased at the beginning of immersion, until they reached a plateau stage. When the coated samples being immersed, the SBF would progressively permeate the coatings, and the potential of the samples decreased. The protection of the coatings delayed the corrosion process of the magnesium substrate, and led to a higher corrosion potential than that of the bare MgZn sample.

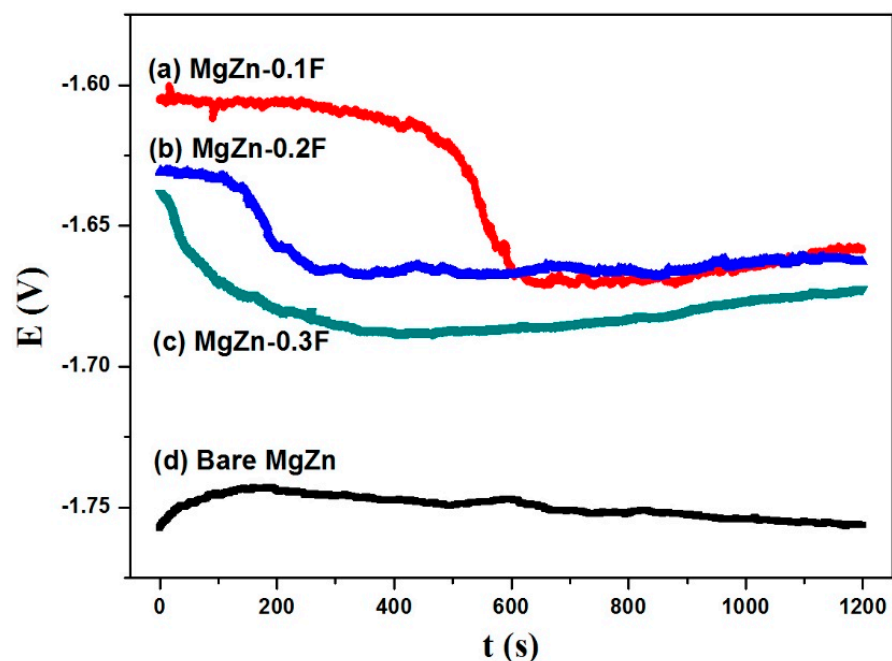


Figure 7. Open-circuit potential (OCP) curves of: (a) MgZn–0.1 F; (b) MgZn–0.2 F; (c) MgZn–0.3 F; (d) bare MgZn substrate.

It should be noted that the trend of the OCP curves was distinguishing between the anatase-coated samples. For the MgZn–0.1 F sample, due to the better protection by a compact coating, the OCP curve decreased more slowly than that of the MgZn–0.2 F and MgZn–0.3 F samples. We believe that the low permeability of the dense coating caused by the high densification of the anatase sheets is the major reason of the high level and the slow decrease of the OCP curve. Therefore, based on the above results and discussion, it can be inferred that the corrosion tendency of the samples is decreased with the densification of the coatings, at similar hydrophilicity as shown in Figure 6.

Figure 8a reveals the platelets adhesion to the bare MgZn alloy. The MgZn alloy was corroded by the plasma and the platelets were aggregated together on the surface of the sample. For the anatase-coated sample, the surface was not corroded due to the protection of the coating. A lower number of platelets were adhered on the surface of the MgZn–0.2 F sample, and the agglomeration of the adhered platelets did not exist. However, some platelets had been deformed and the parapodium had stretched out, which implied that the fixed platelets were activated (see in Figure 8b). Thus, it is hard to decide whether or not the coating has the effect of anti-thrombosis. At least the coatings exhibit the inhibition of platelet aggregation.

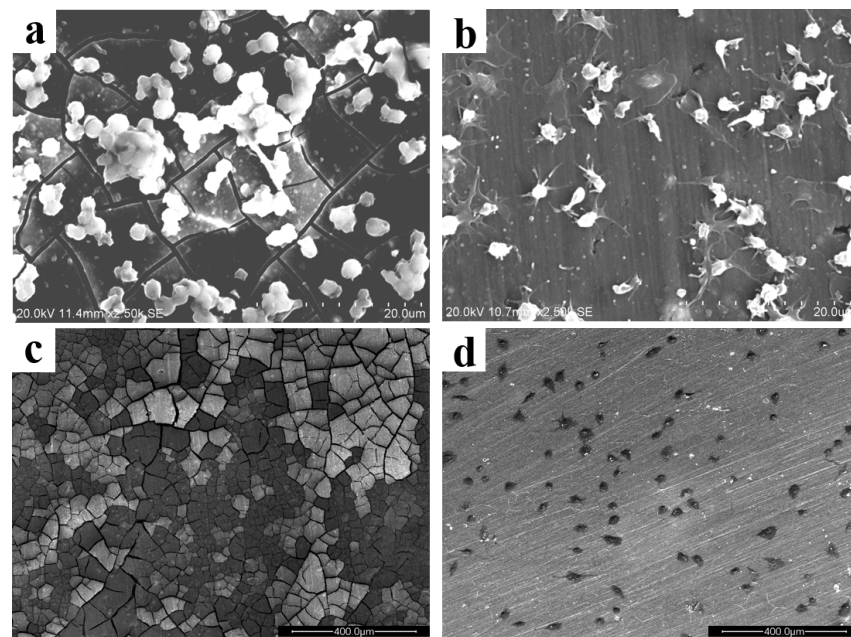


Figure 8. Morphology of adherent platelets on (a) MgZn substrate, (b) MgZn–0.2 F sample; and adherent Ea.hy926 cells on (c) MgZn substrate, (d) MgZn–0.2 F sample.

A layer of endothelial cells has been considered as an anticoagulant surface. For cardiovascular stents, if an endothelial cells layer forms quickly on the surface, the risk of clot formation and restenosis in stents could be significantly reduced. As is known, endothelialization can be influenced by the surface on which the endothelial cells attach. Figure 8c,d shows the morphologies of Ea.hy926 cells cultured on the samples for 1 day. On the bare MgZn surface, endothelial cells were not observed (see Figure 8c). However, for the coated sample, it is seen that many Ea.hy926 cells attached on the surface, and spread in a spindle shape, as presented in Figure 8d. The contact angles of the anatase-coated samples were lower than 20° (see Figure 6), and thus the as-prepared coatings can be considered as hydrophilic surfaces. Generally speaking, materials with a rough and hydrophilic surface are more conducive to cell adhesion. Moreover, due to the fact that the corrosion resistance of the MgZn substrate was improved greatly by the anatase coating, the coated sample was more stable in the Dulbecco's modified Eagle medium and more conducive to cell growth. The results suggest that the anatase coatings with micro/nano-characteristic could enhance the adhesion of endothelial cells and promote re-endothelialization, thus preventing the formation of ISR.

4. Conclusions

The major conclusions of the present work are summarized as follows.

- (1) The surface topography of anatase coating could be controlled in the micro- and nanometer range by the solvothermal method. The anatase coatings were composed of anatase sheets with a thickness of 10–20 nm, and the anatase nanosheets were agglomerated with varying degrees of density. With the increase of NH_4F concentration in the solvothermal solution, the anatase nanosheets were more dispersed, and the surface roughness (R_a) was increased from 49.7 to 90.1 nm. The contact angles of MgZn–0.1 F, MgZn–0.2 F, and MgZn–0.3 F samples were 13.02° , 17.14° , and 16.73° , indicating good hydrophilicity of the anatase coatings.
- (2) After being coated with the anatase coatings, the corrosion resistance of the bare MgZn alloy substrate was improved. Additionally, the corrosion tendency was decreased with the increasing agglomeration density of the anatase nanosheets in the coatings.

- (3) The bare MgZn alloys caused serious platelet aggregation, yet the anatase-coated sample adsorbed a smaller number of platelets, and did not lead to the agglomeration of the adhered platelets. After being coated with anatase, the samples can adsorb endothelial cells on the surface, which maybe promote the re-endothelialization of stents.

Author Contributions: Conceptualization, S.H. and L.Y.; methodology, W.Y.; formal analysis, L.L. and S.H.; writing—original draft preparation, T.Y. and Y.L.; writing—review and editing, W.Y. and S.H. All authors have read and agreed to the published version of the manuscript.

Funding: This research was funded by Key Research and Development Specialized Project of Henan Province (Grant No. 182102210120, 222102230023) and Key Scientific Research Project of College and University of Henan Province (Grant No. 22A430035).

Institutional Review Board Statement: Not applicable.

Informed Consent Statement: Not applicable.

Data Availability Statement: Not applicable.

Conflicts of Interest: The authors declare no conflict of interest.

References

1. Cho, Y.C.; Hung, W.C.; Lan, W.C.; Saito, T.; Huang, B.H.; Lee, C.H.; Tsai, H.Y.; Huang, M.S.; Ou, K.L. Anodized Biomedical Stainless-Steel Mini-Implant for Rapid Recovery in a Rabbit Model. *Metals* **2021**, *11*, 1575. [[CrossRef](#)]
2. Ho, M.Y.; Chen, C.C.; Wang, C.Y.; Chang, S.H.; Hsieh, M.J.; Lee, C.H.; Wu, V.; Hsieh, I.C. The Development of Coronary Artery Stents: From Bare-Metal to Bio-Resorbable Types. *Metals* **2016**, *6*, 168. [[CrossRef](#)]
3. Rout, P.K.; Roy, S.; Ganguly, S.; Rathore, D.K. A review on properties of magnesium-based alloys for biomedical applications. *Biomed. Phys. Eng. Express*. **2022**, *8*, 042002. [[CrossRef](#)] [[PubMed](#)]
4. Chagnon, M.; Guy, L.G.; Jackson, N. Evaluation of Magnesium-based Medical Devices in Preclinical Studies: Challenges and Points to Consider. *Toxicol. Pathol.* **2019**, *47*, 390–400. [[CrossRef](#)] [[PubMed](#)]
5. Zhang, D.; Liu, Y.; Liu, Z.; Wang, Q. Advances in Antibacterial Functionalized Coatings on Mg and Its Alloys for Medical Use—A Review. *Coatings* **2020**, *10*, 828. [[CrossRef](#)]
6. Soleymani, F.; Emadi, R.; Sadeghzade, S.; Tavangarian, F. Bioactivity Behavior Evaluation of PCL-Chitosan-Nanobaghdadite Coating on AZ91 Magnesium Alloy in Simulated Body Fluid. *Coatings* **2020**, *10*, 231. [[CrossRef](#)]
7. Gu, X.N.; Guo, H.M.; Wang, F.; Lu, Y.; Lin, W.T.; Li, J.; Zheng, Y.F.; Fan, Y.B. Degradation, hemolysis, and cytotoxicity of silane coatings on biodegradable magnesium alloy. *Mater. Lett.* **2017**, *193*, 266–269. [[CrossRef](#)]
8. Echeverry-Rendon, M.; Allain, J.P.; Robledo, S.M.; Echeverria, F.; Harmsen, M.C. Coatings for biodegradable magnesium-based supports for therapy of vascular disease: A general view. *Mater. Sci. Eng. C Mater.* **2019**, *102*, 150–163. [[CrossRef](#)]
9. Rourke, A.S.; Beard, M.C.; Jones, S.E.; Priddy, M.W.; Priddy, L.B. Hydroxyapatite coating promotes stable physicochemical properties of pure magnesium in a longitudinal degradation study. *J. Mater. Res.* **2022**, *37*, 1231–1245. [[CrossRef](#)]
10. Zhang, Q.; Zhang, L.; Yang, M.; Hong, Q.; Yang, Z.; Liu, S.; Xiong, Q.; Pan, C. Construction of Chi(Zn/BMP2)/HA composite coating on AZ31B magnesium alloy surface to improve the corrosion resistance and biocompatibility. *Nanotechnol. Rev.* **2021**, *10*, 870–882. [[CrossRef](#)]
11. Ben-Yehuda, O. Long-Term Outcomes with Drug-Eluting Stents: Beyond Stent Choice. *J. Am. Coll. Cardiol.* **2020**, *76*, 159–161. [[CrossRef](#)] [[PubMed](#)]
12. Dong, H.; Li, D.; Mao, D.; Bai, N.; Chen, Y.; Li, Q. Enhanced performance of magnesium alloy for drug-eluting vascular scaffold application. *Appl. Surf. Sci.* **2018**, *435*, 320–328. [[CrossRef](#)]
13. Liu, J.; Zheng, B.; Wang, P.; Wang, X.; Zhang, B.; Shi, Q.; Xi, T.; Chen, M.; Guan, S. Enhanced in Vitro and in Vivo Performance of Mg-Zn-Y-Nd Alloy Achieved with APTES Pretreatment for Drug-Eluting Vascular Stent Application. *ACS Appl. Mater. Interfaces* **2016**, *8*, 17842–17858. [[CrossRef](#)] [[PubMed](#)]
14. Hou, S.; Yu, W.; Yang, Z.; Li, Y.; Yang, L.; Lang, S. Properties of Titanium Oxide Coating on MgZn Alloy by Magnetron Sputtering for Stent Application. *Coatings* **2020**, *10*, 999. [[CrossRef](#)]
15. Ramos-Corella, K.J.; Sotelo-Lerma, M.; Gil-Salido, A.A.; Rubio-Pino, J.L.; Auciello, O.; Quevedo-López, M.A. Controlling crystalline phase of TiO₂ thin films to evaluate its biocompatibility. *Mater. Technol.* **2019**, *34*, 455–462. [[CrossRef](#)]
16. Hou, S.S.; Zhang, R.R.; Guan, S.K.; Ren, C.X.; Gao, J.H.; Lu, Q.B.; Cui, X.Z. In vitro corrosion behavior of Ti-O film deposited on fluoride-treated Mg-Zn-Y-Nd alloy. *Appl. Surf. Sci.* **2012**, *258*, 3571–3577. [[CrossRef](#)]
17. Liang, C.; Hu, Y.; Wang, H.; Xia, D.; Li, Q.; Zhang, J.; Yang, J.; Li, B.; Li, H.; Han, D.; et al. Biomimetic cardiovascular stents for in vivo re-endothelialization. *Biomaterials* **2016**, *103*, 170–182. [[CrossRef](#)]
18. Liu, T.; Liu, S.; Zhang, K.; Chen, J.; Huang, N. Endothelialization of implanted cardiovascular biomaterial surfaces: The development from in vitro to in vivo. *J. Biomed. Mater. Res. A* **2014**, *102*, 3754–3772. [[CrossRef](#)]

19. Guo, X.; Wang, X.; Li, X.; Jiang, Y.C.; Han, S.; Ma, L.; Guo, H.; Wang, Z.; Li, Q. Endothelial Cell Migration on Poly(epsilon-caprolactone) Nanofibers Coated with a Nanohybrid Shish-Kebab Structure Mimicking Collagen Fibrils. *Biomacromolecules* **2020**, *21*, 1202–1213. [[CrossRef](#)]
20. Cutiongco, M.F.A.; Goh, S.H.; Aid-Launais, R.; Le Visage, C.; Low, H.Y.; Yim, E.K.F. Planar and tubular patterning of micro and nano-topographies on poly(vinyl alcohol) hydrogel for improved endothelial cell responses. *Biomaterials* **2016**, *84*, 184–195. [[CrossRef](#)]
21. Bedair, T.M.; ElNaggar, M.A.; Joung, Y.K.; Han, D.K. Recent advances to accelerate re-endothelialization for vascular stents. *J. Tissue Eng.* **2017**, *8*. [[CrossRef](#)] [[PubMed](#)]
22. Jana, S. Endothelialization of cardiovascular devices. *Acta Biomater.* **2019**, *99*, 53–71. [[CrossRef](#)]
23. Hou, S.; Mi, L.; Wang, L.; Zhu, S.; Hu, J.; Ding, Q.; Guan, S. Corrosion protection of Mg-Zn-Y-Nd alloy by flower-like nanostructured TiO₂ film for vascular stent application. *J. Chem. Technol. Biot.* **2013**, *88*, 2062–2066. [[CrossRef](#)]
24. Hou, S. Solvothermal fabrication of TiO₂ nanosheet films on degradable Mg-Zn alloys. *Surf. Eng.* **2016**, *32*, 745–749. [[CrossRef](#)]
25. Wang, J.; Wang, L.; Guan, S.; Zhu, S.; Ren, C.; Hou, S. Microstructure and corrosion properties of as sub-rapid solidification Mg-Zn-Y-Nd alloy in dynamic simulated body fluid for vascular stent application. *J. Mater. Sci. Mater. Med.* **2010**, *21*, 2001–2008. [[CrossRef](#)]
26. Kokubo, T.; Takadama, H. How useful is SBF in predicting in vivo bone bioactivity? *Biomaterials* **2006**, *27*, 2907–2915. [[CrossRef](#)]
27. Lu, Y.; Wang, G.; Zhang, H.; Zhang, Y.; Kang, S.; Zhao, H. Photoelectrochemical manifestation of intrinsic photoelectron transport properties of vertically aligned {001} faceted single crystal TiO₂ nanosheet films. *RSC Adv.* **2015**, *5*, 55438–55444. [[CrossRef](#)]
28. Yang, H.G.; Sun, C.H.; Qiao, S.Z.; Zou, J.; Liu, G.; Smith, S.C.; Cheng, H.M.; Lu, G.Q. Anatase TiO₂ single crystals with a large percentage of reactive facets. *Nature* **2008**, *453*, 638–641. [[CrossRef](#)]
29. Hallab, N.J.; Bundy, K.J.; O'Connor, K.; Moses, R.L.; Joshua, J.; Jacobs, J.J. Evaluation of Metallic and Polymeric Biomaterial Surface Energy and Surface Roughness Characteristics for Directed Cell Adhesion. *Tissue Eng.* **2001**, *7*, 55–71. [[CrossRef](#)]